DALTON
FULL PAPER

# A dimolybdenum complex with an alkyne ligand parallel to the metal–metal bond: synthesis, structure and cluster formation reactions of $[Mo_2(\mu\text{-}\eta^1,\eta^1\text{-}C_2Ph_2)(\mu\text{-}S)(\mu\text{-}SPr^i)_2Cp_2]$

**Harry Adams,[a] Michael J. Morris,*[a] Philip Mountford,*[b] Rushmiben Patel[a] and Sharon E. Spey[a]**

[a] *Department of Chemistry, University of Sheffield, Sheffield, UK S3 7HF*
[b] *Inorganic Chemistry Laboratory, South Parks Road, University of Oxford, Oxford, UK OX1 3QR*

***Received 24th April 2001, Accepted 11th July 2001***
***First published as an Advance Article on the web 21st August 2001***

The dimolybdenum alkyne complex $[Mo_2(\mu\text{-}C_2Ph_2)(CO)_4Cp_2]$ **1** (Cp = $\eta$-$C_5H_5$), in which the alkyne ligand is perpendicular to the Mo–Mo bond, reacts with $Pr^iSH$ to afford two separable isomers of $[Mo_2(\mu\text{-}\eta^1,\eta^1\text{-}C_2Ph_2)(\mu\text{-}S)(\mu\text{-}SPr^i)_2Cp_2]$ **2** in which the alkyne lies parallel to the Mo–Mo bond. In crystallographically characterised **2a** the $Pr^i$ substituents are both directed away from the alkyne ligand in a *syn* arrangement, creating a plane of symmetry, whereas in unsymmetrical **2b** they are presumed to occupy an *anti* arrangement. Extended-Hückel molecular orbital calculations show that the alkyne orientation in **2** results in better overlap between the alkyne and metal orbitals, as well as reduced repulsive interactions with the bridging thiolate ligands. Both isomers of **2** react with $[Ru_3(CO)_{12}]$ to afford the same two products: the tetrahedral cluster $[Mo_2Ru_2(\mu_3\text{-}C_2Ph_2)(\mu_3\text{-}S)(\mu\text{-}SPr^i)_2(CO)_4Cp_2]$ **7** in which the alkyne ligand remains parallel to the Mo–Mo edge, and trinuclear $[Mo_2Ru(\mu\text{-}C_2Ph_2)(\mu_3\text{-}S)_2(CO)_3Cp_2]$ **8** in which the alkyne has resumed its original perpendicular orientation; the crystal structures of both clusters are reported.

## Introduction

The removal of sulfur-containing impurities from crude oil by the hydrodesulfurisation (HDS) reaction is considered to be the most widely practiced example of industrial heterogeneous catalysis.[1] With environmental concerns constantly lowering the acceptable sulfur content of refined fuel, increased efficiency of the process is needed, especially given that future crude oil stocks may contain higher initial levels of sulfur. The catalyst currently employed consists of molybdenum sulfide with a cobalt sulfide promoter, supported on an inert material such as alumina. Various models have been proposed for the mechanism of sulfur removal and the role within it of hydrogenation reactions which are also catalysed under the conditions used. In order to elucidate the mechanism of the processes occurring on the catalyst surface, molecular molybdenum–sulfur complexes and heterometallic clusters derived from them have been used as model systems. For example, Curtis and co-workers have shown that the desulfurisation reaction can be modelled successfully on Mo–Co clusters, in particular $[Mo_2Co_2(\mu_3\text{-}S)_2(\mu_4\text{-}S)(CO)_4Cp_2]$ which can abstract sulfur from a variety of organic species to afford the cubane cluster $[Mo_2Co_2(\mu_3\text{-}S)_4(CO)_2Cp_2]$ in a stoichiometric manner.[2] It is however known that other late transition metals, particularly ruthenium, are equally if not more effective as promoters of the HDS reaction, and we are therefore investigating the synthesis of Mo–Ru clusters with sulfur ligands.

In a series of recent papers, we have examined the reactions of the dimolybdenum alkyne complexes $[Mo_2(\mu\text{-}R^1C_2R^2)(CO)_4Cp_2]$ with thiols $R^3SH$ (and other sulfur-containing organics) as possible routes to new and known dimolybdenum complexes with sulfur-based ligand systems.[3,4] The products are heavily influenced by the identity of the substituents $R^1$–$R^3$. For example, if $R^2$ is $CO_2Me$, μ-vinyl complexes of the type $[Mo_2(\mu\text{-}CR^1{=}CHCO_2Me)(\mu\text{-}SR^3)(CO)_2Cp_2]$, stabilised by coordination of the β-carboxylate group to Mo, can be isolated, except in the case where $R^1 = R^2 = CO_2Me$ and $R^3 = Bu^t$, where the unusual sulfur-bridged alkene complex $[Mo_2(\mu\text{-}S)_2(\mu\text{-}MeO_2CCH{=}CHCO_2Me)Cp_2]$ is formed.[3] If $R^1 = R^2 = Me$ (or most other combinations of H or alkyl groups), reasonable yields of the known quadruply-bridged species $[Mo_2(\mu\text{-}S)_2(\mu\text{-}SR^3)_2Cp_2]$ are produced, though again $Bu^tSH$ differs in yielding the vinyl complex $[Mo_2(\mu\text{-}CMe{=}CHMe)(\mu\text{-}SBu^t)(CO)_3Cp_2]$.[4] In this paper we describe the synthesis and structure of a novel type of complex which can as yet only be isolated from the reaction of $[Mo_2(\mu\text{-}C_2Ph_2)(CO)_4Cp_2]$ **1** with $Pr^iSH$, and show that it can serve as the precursor to further new mixed-metal (Mo–Ru) clusters.

## Results and discussion

### Synthesis and X-ray crystal structure of $[Mo_2(\mu\text{-}\eta^1,\eta^1\text{-}C_2Ph_2)(\mu\text{-}S)(\mu\text{-}SPr^i)_2Cp_2]$ 2

Reaction of $[Mo_2(\mu\text{-}C_2Ph_2)(CO)_4Cp_2]$ **1** with an excess of $Pr^iSH$ in refluxing toluene for 18 h affords the new complex **2** as two separable isomers, symmetrical **2a** and unsymmetrical **2b**, in a combined yield of 40% (Scheme 1). Thus, in the $^1H$ NMR

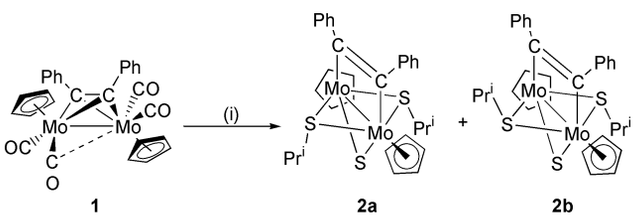


**Scheme 1** Synthesis of the two isomers of complex **2**. Reagents and conditions: (i) $Pr^iSH$ (5 equivalents), toluene, reflux, 18 h.

spectrum of **2a**, the two $Pr^i$ groups are equivalent and appear as a septet and a doublet whereas for **2b** two septets and two doublets are observed. Each isomer has equivalent Cp ligands,

DOI: 10.1039/b103698j

**Table 1** Selected bond lengths [Å] and angles [°] for complex **2a**

| | | | |
|---|---|---|---|
| Mo(1)–C(1) | 2.108(5) | Mo(1)–S(3) | 2.3455(15) |
| Mo(1)–S(2) | 2.4539(14) | Mo(1)–S(1) | 2.4699(14) |
| Mo(1)–Mo(2) | 2.6839(7) | Mo(2)–C(2) | 2.104(6) |
| Mo(2)–S(3) | 2.3457(15) | Mo(2)–S(1) | 2.4530(15) |
| Mo(2)–S(2) | 2.4684(14) | C(1)–C(2) | 1.380(8) |
| | | | |
| C(1)–Mo(1)–S(3) | 127.17(17) | C(1)–Mo(1)–S(2) | 74.03(15) |
| S(3)–Mo(1)–S(2) | 76.90(5) | C(1)–Mo(1)–S(1) | 75.34(15) |
| S(3)–Mo(1)–S(1) | 76.61(5) | S(2)–Mo(1)–S(1) | 112.60(5) |
| C(1)–Mo(1)–Mo(2) | 72.07(17) | S(3)–Mo(1)–Mo(2) | 55.11(4) |
| S(2)–Mo(1)–Mo(2) | 57.22(3) | S(1)–Mo(1)–Mo(2) | 56.66(4) |
| C(2)–Mo(2)–S(3) | 126.90(15) | C(2)–Mo(2)–S(1) | 73.65(15) |
| S(3)–Mo(2)–S(1) | 76.94(5) | C(2)–Mo(2)–S(2) | 75.46(14) |
| S(3)–Mo(2)–S(2) | 76.61(5) | S(1)–Mo(2)–S(2) | 112.69(5) |
| C(2)–Mo(2)–Mo(1) | 71.81(14) | S(3)–Mo(2)–Mo(1) | 55.10(4) |
| S(1)–Mo(2)–Mo(1) | 57.27(4) | S(2)–Mo(2)–Mo(1) | 56.70(3) |
| Mo(2)–S(1)–Mo(1) | 66.07(4) | Mo(1)–S(2)–Mo(2) | 66.08(4) |
| Mo(1)–S(3)–Mo(2) | 69.79(4) | C(2)–C(1)–C(13) | 124.5(5) |
| C(2)–C(1)–Mo(1) | 107.6(4) | C(1)–C(2)–C(19) | 122.2(5) |
| C(1)–C(2)–Mo(2) | 108.4(4) | | |

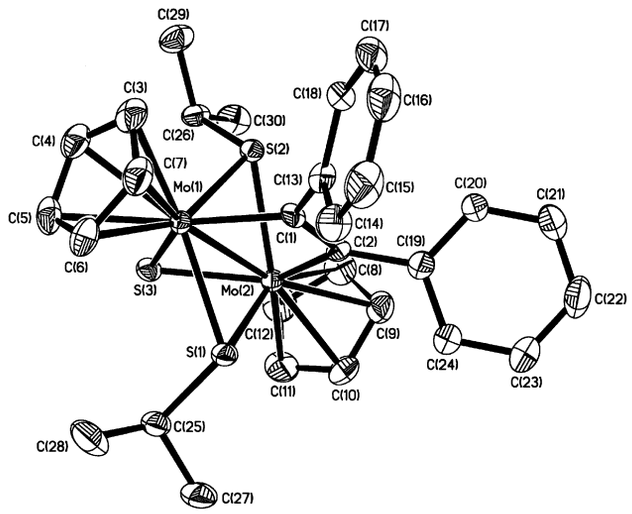


**Fig. 1** Molecular structure of *syn*-$[Mo_2(\mu\text{-}\eta^1,\eta^1\text{-}C_2Ph_2)(\mu\text{-}S)(\mu\text{-}SPr^i)_2Cp_2]$ **2a** in the crystal showing the atomic numbering scheme.

and the fact that even in **2b** the phenyl groups and the alkyne carbons are equivalent in the $^1H$ and $^{13}C$ NMR spectra implies that the alkyne ligand lies parallel to the metal–metal bond; moreover the $^{13}C$ chemical shifts of the alkyne carbons were unusually high ($\delta$ 242.4 for **2a**, 254.3 for **2b**). The absence of carbonyl peaks in the IR spectra confirmed that complete decarbonylation of the dimolybdenum centre had occurred, and mass spectrometry indicated the presence of an additional sulfur atom, which presumably arises through the dealkylation of a further $SPr^i$ unit. We therefore formulated **2** as $[Mo_2(\mu\text{-}\eta^1,\eta^1\text{-}C_2Ph_2)(\mu\text{-}S)(\mu\text{-}SPr^i)_2Cp_2]$, with the view that in **2a**, both $Pr^i$ substituents are arranged in a *syn* orientation (pointing away from the bulky alkyne ligand on steric grounds) and in **2b** they are in an *anti* orientation and are therefore inequivalent. As observed previously with the *syn* and *anti* isomers of $[Mo_2(\mu\text{-}S)_2(\mu\text{-}SR)_2Cp_2]$ **3**, no interconversion between **2a** and **2b** was detected in solution, *i.e.* the barrier to sulfur inversion is high.

Obtaining crystals of one of the isomers for X-ray diffraction was complicated by their high solubilities in hydrocarbon solvents, but eventually a suitable crystal of **2a** was grown by diffusion of ethanol into a solution in light petroleum. The structure is shown in Fig. 1, with selected bond lengths and angles collected in Table 1. The two molybdenum atoms, each of which is in a square-based pyramidal environment, are joined by a bond of length 2.6839(7) Å, which, if each metal atom is to attain an 18-electron configuration, could *formally* be regarded as a double bond (but see the discussion of the bonding below). The bond is bridged by four ligands which form the familiar orthogonal motif already observed in complexes such as $[Mo_2(\mu\text{-}S)_2(\mu\text{-}SR)_2Cp_2]$ **3**[5] and $[Mo_2(\mu\text{-}S)_2(\mu\text{-}SPr^i)(\mu\text{-}PPh_2)Cp_2]$ **4**[6] and more recently in the trithiocarbonate-derived compounds $[Mo_2(\mu\text{-}S)(\mu\text{-}SCR{=}CRSCCR{=}CR)Cp_2]$[7] and $[Mo_2(\mu\text{-}S)(\mu\text{-}SMe)\{\mu\text{-}CRC(SMe)CR\}Cp_2]$ (R = $CO_2Me$).[8] In the present case, three of the bridging positions are occupied by a symmetrically bound sulfido ligand and two slightly asymmetrically bound $SPr^i$ groups: S(1) is slightly closer to Mo(2) and conversely S(2) slightly closer to Mo(1). The $Pr^i$ substituents of the thiolate ligands are both directed towards S(3) and away from the bulky diphenylacetylene. The latter is the major focus of interest, as it lies parallel to the Mo–Mo bond [the torsion angle of the C(1)–C(2) bond with respect to the Mo(1)–Mo(2) bond is 3.0°] and has therefore undergone a 90° rotation from its original perpendicular orientation in **1**.[9] The bending back angles of the phenyl substituents, C(2)–C(1)–C(13) and C(1)–C(2)–C(19), are 124.5(5) and 122.2(5)° respectively, typical of alkynes bound in this fashion.[10] The Mo(1)–C(1) and Mo(2)–C(2) bond lengths [2.108(5) and 2.104(6) Å respectively] are both relatively short, perhaps indicating the presence of some degree of multiple bonding, though the C(1)–C(2) distance of 1.380(8) Å is consistent with a double bond. We therefore propose that the alkyne is bonded as a dianionic 2-electron donor, essentially as a dimetallated alkene, as opposed to a possible alternative formulation as a bis-alkylidene ligand with a C–C single bond. Thus, **2** can be thought of as derived from $[Mo_2(\mu\text{-}S)_2(\mu\text{-}SR)_2Cp_2]$ by replacement of one of the $S^{2-}$ groups by a $C_2Ph_2^{2-}$ ligand, and the molybdenum atoms can be considered as Mo(IV), a view reinforced by the molecular orbital calculations reported below.

## Molecular orbital analysis of complex 2

**Introductory remarks.** It appears that **2** is the first example of a dimolybdenum complex with an alkyne ligand bonded in the parallel $\mu\text{-}\eta^1,\eta^1$ mode, which is more common for later transition metals such as Ru, Rh and Ir. For Group 6 metals, the perpendicular mode (seen in **1**) is almost universal, though there are a small number of compounds where a skewed alkyne orientation is observed, ranging from the aminoalkyne complex $[Mo_2(\mu\text{-}Et_2NC_2NEt_2)(CO)_4Cp_2]$[11] to the tungsten species $[W_2Cl_4(NMe_2)_2(\mu\text{-}C_2Me_2)(py)_2]$,[12] $[W_2(\mu\text{-}C_2H_2)(\mu\text{-}OR)_2(OR)_6]$ (R = neopentyl),[13] and $[W_2Br_4(\mu\text{-}C_2Ph_2)(\eta\text{-}C_5H_4Pr^i)_2]$,[14] some of which have been analysed theoretically.

We have therefore investigated the bonding in **2** at the extended-Hückel molecular orbital (EHMO) theory level.[15] This method has enjoyed widespread success in the past in analysing the bonding and alkyne orientation preferences in a broad range of binuclear μ-alkyne complexes.[10,12–14,16–18] General analyses of the bonding in such μ-alkyne complexes have been reported previously.[10] A particularly useful strategy in such systems is to use the fragment orbital approach in which the orbitals of a *cis*-bent alkyne are allowed to interact with those of a dimetallic moiety. This is the approach taken here for $[Mo_2(\mu\text{-}\eta^1,\eta^1\text{-}C_2H_2)(\mu\text{-}S)(\mu\text{-}SH)_2Cp_2]$ **I** and $[Mo_2(\mu\text{-}\eta^2,\eta^2\text{-}C_2H_2)(\mu\text{-}S)(\mu\text{-}SH)_2Cp_2]$ **II** (Fig. 2). The compound **I** is a model for the real complex **2** with the alkyne bound parallel to the Mo–Mo vector; distances and angles are based on those of **2**, idealised to $C_{2v}$ symmetry with the $Pr^i$ and Ph groups modelled by H atoms for computational simplicity. The compound **II** is a model of the hypothetical perpendicular bridged alkyne isomer of **2**. To aid comparisons between the two models, in the first instance distances and angles in **II** are exactly as in **I**, except that the C–C bond of the $\mu\text{-}C_2H_2$ ligand is perpendicular in projection onto the Mo–Mo vector. Thus **II** has the mid-point of the $C_2H_2$ lying 2.00 Å above that of the Mo–Mo bond; this gives Mo–$C_{ac}$ distances of 2.51 Å.

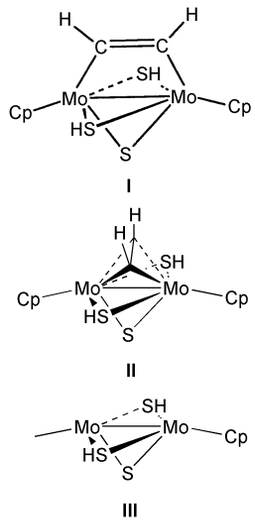


**Fig. 2** Structures of the species used in the EHMO analysis.

**Orbitals of the $[Mo_2(\mu\text{-}S)(\mu\text{-}SH)_2Cp_2]$ III and *cis*-bent $C_2H_2$ fragments.** Interaction diagrams between the frontier orbitals of the fragments $[Mo_2(\mu\text{-}S)(\mu\text{-}SH)_2Cp_2]$ **III** and *cis*-bent $C_2H_2$ are shown in Figs. 3 and 4 for **I** and **II**, respectively. The derivation and nature of the frontier orbitals of *cis*-bent $C_2H_2$, which are shown on the right of these figures, have been described in detail elsewhere.[10,18] They transform as (in order of increasing stability) $a_2 + b_1$ (or $b_2$) + $a_1 + b_2$ (or $b_1$) under the $C_{2v}$ symmetry of both the fragment and the resultant complex. For convenience, they will be referred to herein as (in order of increasing stability) $\pi^*(\perp)$, $\pi^*(||)$, $\pi(\perp)$ and $\pi(||)$ ($\perp$ and $||$ indicate whether the $\pi/\pi^*$ MOs are perpendicular or parallel to the $C_2H_2$ plane). The orbitals of the $C_{2v}$ fragment **III** have not been reported elsewhere but are readily traced to those for related complexes $[Mo_2(\mu\text{-}SH)_4Cp_2]$, $[Mo_2(\mu\text{-}S)_2(\mu\text{-}SH)_2Cp_2]$, $[Mo_2(\mu\text{-}S)_4Cp_2]$ (a hypothetical species since lone-pair repulsions between the μ-sulfurs lead to the isomeric $[Mo_2(S)_2(\mu\text{-}S)_2Cp_2]$) and $[Mo_2(\mu\text{-}Cl)_4Cp_2]$ which have all been analyzed before at the EHMO level.[19–21]

There are three occupied, metal-based MOs of **III** (at the left of Figs. 3 and 4). These are the $2a_1$ (Mo–Mo σ bonding), $1a_2$ (Mo–Mo δ* anti-bonding) and $2b_2$ (Mo–Mo δ bonding). That the $1a_2$ (δ*) level lies below $2b_2$ (δ) is at first sight counter-intuitive, but is readily accounted for by the small but significant π* anti-bonding interaction between the in-phase 4d(*yz*) AOs (that make up the δ bonding combination) and the μ-S 3p(*z*) AO that contributes to this $2b_2$ MO. Analogous reversals of the expected δ < δ* MO level orderings are found for the all tetra-bridged systems mentioned above.[19–21] The fragment **III** therefore has a $d^3$–$d^3$ manifold with the configuration $\sigma^2\,(\delta^*)^2\,\delta^2$ giving a formal Mo–Mo single bond. Close in energy to the $d^3$–$d^3$ manifold are the in- and out-of-phase combinations of the μ-SH lone pairs, namely the $1a_1$ and $1b_2$ levels. Again, the prominent presence of μ-ligand lone pairs is reminiscent of the situation found in the tetra-bridged systems above. Close to the $2b_2$ HOMO (highest occupied molecular orbital) lie the $3a_1$ and $1b_1$ MOs. These are derived, in the coordinate system chosen, predominantly from Mo 4d($z^2$) with some 5p(*z*) contribution. These two orbitals are spatially and energetically very well disposed for further metal–ligand bonding interactions; indeed they are the main MOs that will be used for σ-bonding to a fourth bridging group.

**Bonding in the parallel bridged isomer $[Mo_2(\mu\text{-}\eta^1,\eta^1\text{-}C_2H_2)(\mu\text{-}S)(\mu\text{-}SH)_2Cp_2]$ I.** A partial MO interaction scheme for **I** is shown in Fig. 3. Mulliken overlap and orbital populations for all the fragments and compounds are listed in Table 2. The strongest interactions are between the alkyne $\pi(||)$ and $\pi^*(||)$ frontier MOs and the $3a_1$ and $1b_1$ orbitals, respectively, of **III**. In addition to these Mo–$C_{ac}$ σ interactions there are two, weaker, π-interactions. These are between the alkyne $\pi(\perp)$ and $\pi^*(\perp)$ MOs and the **III** fragment $2b_2$ and $1a_2$ MOs. The $\pi(\perp)$–$2b_2$ interaction is formally a 4-electron 2-orbital one, but the resultant $2b_2$ (anti-bonding) MO of **I** is in fact the LUMO in the final complex as the $1b_1$ bonding MO becomes filled. The interaction of the $\pi^*(\perp)$ MO with the $1a_2$ level of **III** stabilises this Mo–Mo δ* anti-bonding orbital. There are several secondary interactions between **III** and the $C_2H_2$ ligand which result in the relatively small destabilisation of the $(\mu\text{-}SH)_2$ lone pairs ($1a_1$ and $1b_2$) as well as the Mo–Mo σ bonding level $2a_1$.

Overall the parallel bonding mode of $C_2H_2$ in **I** gives excellent matches between all four alkyne MOs and fragment **III**. As Table 2 shows this results in substantial transfer of electron density from the $Mo_2$ core to $C_2H_2$ [and in particular to the $\pi^*(||)$ MO]. There is a concomitant reduction in both the $C_{ac}$–$C_{ac}$ and Mo–Mo Mulliken overlap populations in **I** compared to the starting fragments. The orbital description is consistent with the $\mu\text{-}C_2H_2$ ligand in **I** possessing a formal $C_{ac}$–$C_{ac}$ double bond and 2− charge in a valence bond description. The formal Mo–Mo bond order is less obvious. There are now only two filled metal-based MOs in the frontier orbital manifold of **I** suggesting a $d^2$–$d^2$ (*i.e.* Mo(IV)$_2$) description. These are the $1a_2$ (Mo–Mo δ* anti-bonding) and $2a_1$ (Mo–Mo σ-bonding) MOs so it is more appropriate to assign a formal Mo–Mo bond order of ≤1 to **I** than an otherwise apparently possible double bond. Such a position is not without precedent: the formally doubly-bonded ditantalum complex $[Ta_2(\mu\text{-}Cl)_4(\eta\text{-}C_5Me_5)_2]$ ($d^2$–$d^2$) has a frontier MO description $\sigma^2\,(\delta^*)^2$ and therefore does not possess a Ta=Ta double bond.[21]

**Bonding in the perpendicular-bridged isomer $[Mo_2(\mu\text{-}\eta^2,\eta^2\text{-}C_2H_2)(\mu\text{-}S)(\mu\text{-}SH)_2Cp_2]$ II.** Rotating the alkyne by 90° relative to the Mo–Mo vector of **III** has a dramatic effect on the metal–alkyne bonding as revealed by the fragment orbital interaction diagram in Fig. 4. Going from **I** (parallel bridging alkyne) to **II** results in a *ca.* 4.0 eV (*ca.* 387 kJ mol$^{-1}$) *destabilisation* of the complex signalling a substantial electronic preference for the parallel bridging mode found for the real complex **2**. Before considering the orbital interaction diagram it is helpful to examine the Mulliken fragment orbital overlap and populations for **II** (Table 2). The Mo–Mo and $C_{ac}$–$C_{ac}$ overlap populations for **II** are reduced relative to the fragments **III** and *cis*-bent $C_2H_2$ as one would expect. However, compared to the parallel bridged isomer these values are somewhat increased implying a weaker $Mo_2$–alkyne interaction. This is reinforced by the greatly decreased Mo–$C_{ac}$ overlap populations for **II** compared to those in **I**. Also worthy of note are the changes in alkyne π and π* fragment orbital populations on going from **I** to **II**. In the latter the alkyne now acts as a net electron donor to the bimetallic moiety; while there are relatively small changes in the orbital occupancies of the two π donor MOs and the $\pi^*(\perp)$ acceptor level, there is a very large depletion of the alkyne fragment $\pi^*(||)$ MO in **II** compared to that in **I**. Examination of the MO interaction scheme in Fig. 4 shows the origins of all these features which, in turn, arise from the different orientation of the alkyne π and π* MOs relative to those of **III**.

The filled and vacant $\pi(\perp)$ and $\pi^*(\perp)$ MOs of $C_2H_2$ give rise to very good interactions with the fragment **III** orbitals $1b_1$ (vacant) and $1a_2$ (filled Mo–Mo δ*), respectively. The $1a_2$–$\pi^*(\perp)$ interaction is analogous to that in the parallel bridged **I**, stabilising the δ* MO and resulting in a similar $\pi^*(\perp)$ fragment orbital occupation as that for **I**. According to the fragment orbital occupations in Table 2, electron donation from $\pi(\perp)$ to $1b_1$ (a σ-type interaction in **II**) is somewhat more effective than the analogous interaction in **I** [in which donation is from $\pi(\perp)$ to $2b_2$ and hence π-type in nature]. However, the interactions of the $\pi(||)$ and $\pi^*(||)$ MOs of $C_2H_2$ with **III** are altogether less satisfactory. Thus, whereas the $\pi^*(||)$ for the parallel bridging alkyne in **I** found an excellent match (namely $1b_1$) among the

**Table 2** Mulliken overlap and orbital populations ($e^-$) for the model complexes and fragments

| Complex or fragment | Overlap populations | | | Orbital populations | | | | |
|---|---|---|---|---|---|---|---|---|
| | $C_{ac}$–$C_{ac}$ | Mo–Mo | Mo–$C_{ac}$ | π(⊥) | π(\|\|) | π*(\|\|) | π*(⊥) | Net alkyne charge |
| *cis*-bent $C_2H_2$ | 1.570 | — | — | 2.00 | 2.00 | 0.00 | 0.00 | 0.00 |
| **III** | — | 0.233 | — | — | — | — | — | — |
| **I** | 1.208 | 0.138 | 0.618 | 1.75 | 1.48 | 1.18 | 0.16 | −0.42 |
| **II** | 1.264 | 0.173 | 0.161 | 1.59 | 1.41 | 0.40 | 0.13 | 0.61 |
| **IV** | 1.248 | 0.160 | 0.193 | 1.43 | 1.34 | 0.65 | 0.30 | 0.50 |

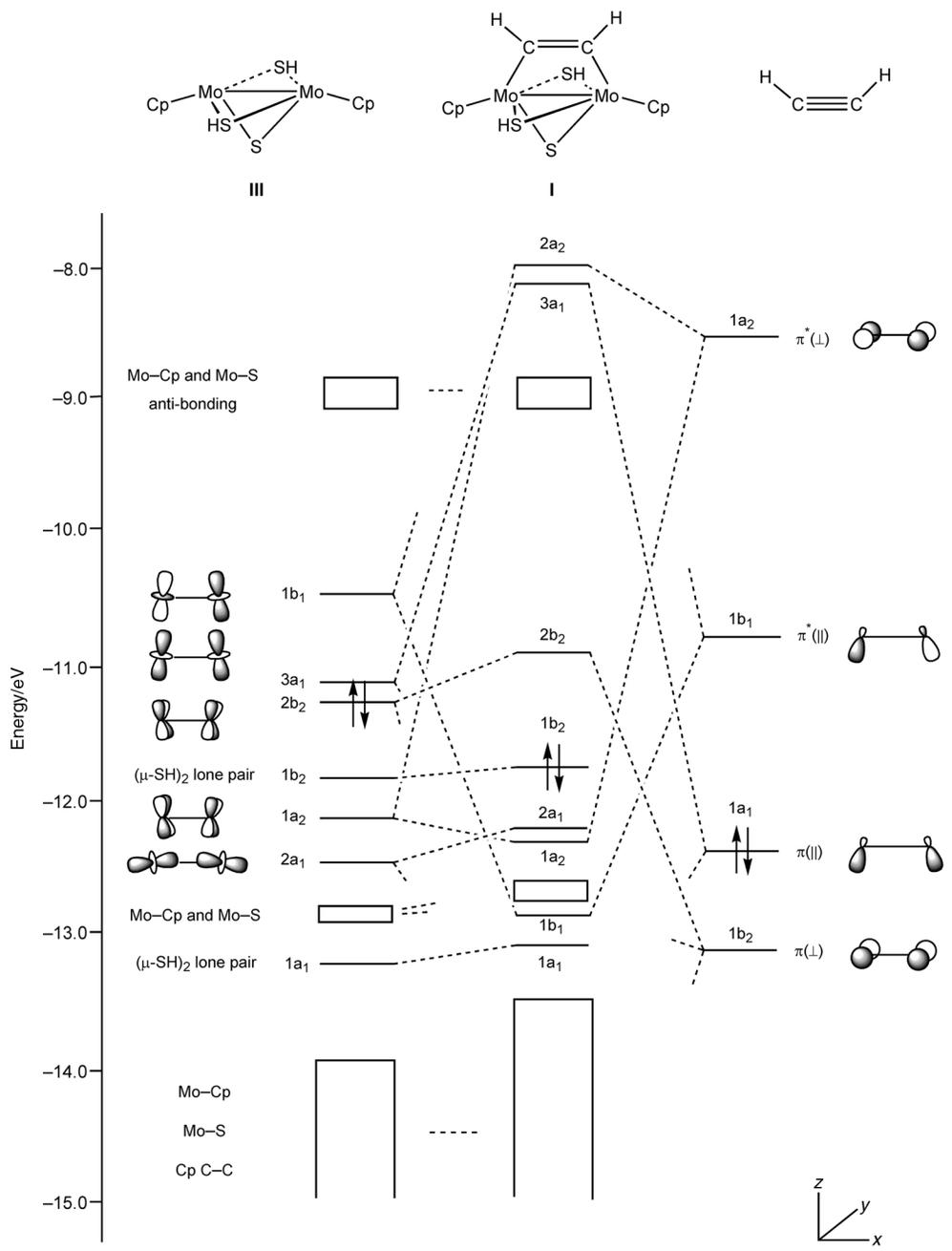


**Fig. 3** Interaction diagram for $[Mo_2(\mu\text{-}S)(\mu\text{-}SH)_2Cp_2]$ **III** with *cis*-bent $C_2H_2$ to give the parallel-bridged isomer $[Mo_2(\mu\text{-}\eta^1,\eta^1\text{-}C_2H_2)(\mu\text{-}S)(\mu\text{-}SH)_2Cp_2]$ **I** The HOMO in each fragment and in the resultant complex is indicated by double arrows.

frontier MOs of **III**, there is no suitable orbital in the case of the perpendicular bridge. In **II** the π*(||) MO has $b_2$ symmetry. There are two filled $b_2$ MOs in the frontier orbital region of **III**. One of these ($1b_2$) has predominantly $(\mu\text{-}SH)_2$ lone pair character, and although there is some interaction between the $1b_2$ MO of **III** and π*(||), it is only a minor one (but sufficient to keep this $1b_2$ sulfur lone pair level in energy on forming **II**). Although the other frontier orbital ($2b_2$: Mo–Mo δ bonding) has a good energy match with π*(||) and is of correct symmetry, the overlap between it and π*(||) is very poor. Thus there is negligible stabilisation of this metal-based MO on forming **II**. The alkyne π*(||) level can in fact interact only with more stable MOs of **III** (not shown in Fig. 4) with which the energy match is relatively poor. This results in poor metal to alkyne back-

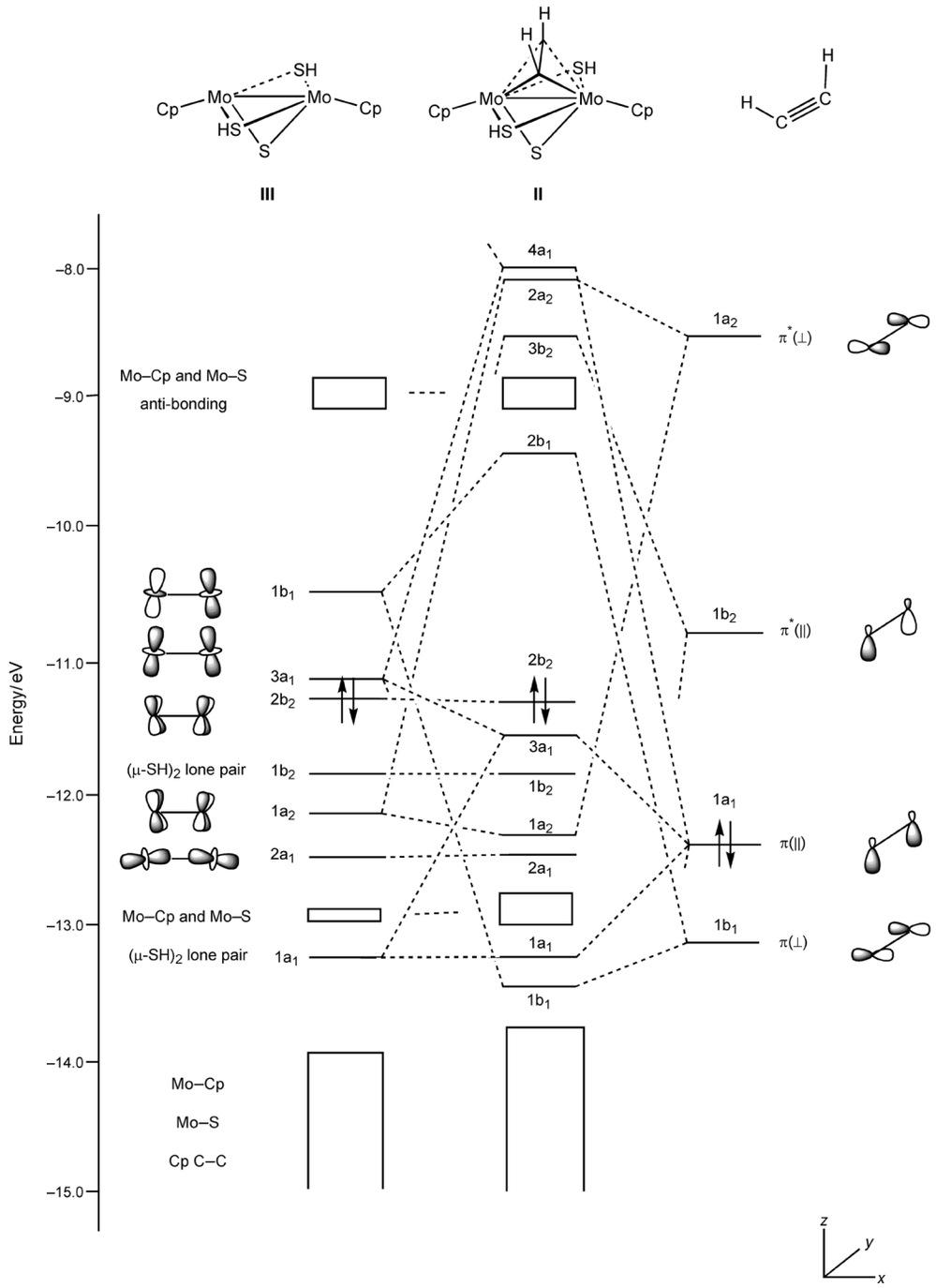


**Fig. 4** Interaction diagram for $[Mo_2(\mu\text{-}S)(\mu\text{-}SH)_2Cp_2]$ **III** with *cis*-bent $C_2H_2$ to give the perpendicular-bridged isomer $[Mo_2(\mu\text{-}\eta^2,\eta^2\text{-}C_2H_2)(\mu\text{-}S)(\mu\text{-}SH)_2Cp_2]$ **II**. The HOMO in each fragment and in the resultant complex is indicated by double arrows.

donation as indicated by the low fragment orbital population of 0.40 e (Table 2).

In **II** the π(||) donor MO of $C_2H_2$ finds a good match with the $3a_1$ LUMO of **III** and the effective resultant alkyne to metal donation is the origin of the reduced (relative to that of free *cis*-bent $C_2H_2$) fragment MO population in Table 2 [this value is comparable to that for π(||) in the parallel bridged complex **I**]. There is little interation between π(||) and the $2a_1$ (Mo–Mo σ-bonding) level due to poor overlap between these MOs. However, there is a significant and destabilising interaction of π(||) with the filled $1a_1$ MO of **III** [mainly the in-phase $(\mu\text{-}SH)_2$ lone pair combination]. The overall result of the overlaps of π(||) (filled) with the $1a_1$ (filled) and $3a_1$ (vacant) MOs of **III** is a 3 centre–4 electron interaction in **II** that keeps the $3a_1$ MO relatively high in energy. Thus the interactions of both π(||) and π*(||) with **III** are much less stabilizing with the alkyne in the perpendicular geometry of **II** than in the parallel bridge arrangement of **I**.

**Further considerations.** Two further issues need to be discussed: (i) Would the perpendicular bridge geometry be more favoured in a model with closer Mo–$C_{ac}$ distances? (ii) How significant are any $(\mu\text{-}SH)_2$ lone pair–alkyne repulsive interactions in the parallel and perpendicular bonded geometries? We address these questions in turn below.

In the previous calculations we transformed **I** into **II** by rotating the alkyne by 90° relative to the Mo–Mo bond while keeping the height of the alkyne above the fragment **III** (*i.e.* distance along the *z* axis) constant at 2.00 Å. This allowed us to analyse the key feaures of the parallel and perpendicular alkyne bonding to **III** with all other geometric parameters constant. However, the Mo–$C_{ac}$ distance of 2.51 Å in **II** is well

outside the usual range of such distances found in structurally authenticated complexes of the general type $[L_nM_2(\mu\text{-}\eta^2,\eta^2\text{-}C_2R_2)]$ (M = Mo, W) where Mo–$C_{ac}$ bond lengths in the range *ca.* 2.0–2.2 Å are typical.[22] Thus a second series of calculations were carried out on a new model complex $[Mo_2(\mu\text{-}\eta^2,\eta^2\text{-}C_2H_2)(\mu\text{-}S)(\mu\text{-}SH)_2Cp_2]$ **IV** which is identical to **II** except that the height of the alkyne above the Mo–Mo vector is now 1.54 Å giving a Mo–$C_{ac}$ distance of 2.15 Å. The MO diagram (not reproduced here) for **IV** is similar in appearance to that for **II**. As expected for tighter alkyne binding,[16] both of the alkyne π* fragment MOs in **IV** have increased Mulliken populations relative to those for **II**. Similarly, the alkyne π (donor) MOs have decreased populations and the overall charge for the alkyne moiety decreases slightly from 0.61 e in **II** to 0.50 e in **IV**. However, the basic deficiencies in the metal–alkyne bonding interactions found for **II** persist in the more tightly bound alkyne model **IV**, and so we should still anticipate that parallel bonding of $C_2H_2$ to **III** would be favoured over the perpendicular alternative. Interestingly, despite the slightly improved metal–alkyne bonding found for **IV** relative to **II**, the calculations found that overall **IV** is 0.82 eV *less* stable (sum of one electron orbital energies) than **II**. This destabilisation reinforces our conclusions concerning the relative stabilities of the perpendicular and parallel bridged geometries and also shows that there are other bonding interactions (apart from metal–alkyne) to consider on going from **II** to **IV**, and possibly from **I** (parallel bridge) to **II**.

The additional bonding features to consider are, of course, repulsive interactions between the $(\mu\text{-}SH)_2$ lone pairs ($1a_1$ and $1b_2$ MOs for **III**) which are oriented "up" towards the alkyne ligand and away from the μ-S ligand. It is well known that lone pair–lone pair repulsive interactions in complexes of the type $[M_2(\mu\text{-}X)_4Cp_2]$ (X = S, SH, halogen) can have important electronic and structural effects[19–21] and so we need to consider their importance for **I**, **II** and **IV**. We have already seen above some specific consequences of this in the interactions of the alkyne π(||) donor MO with *both* the metal-based $3a_1$ *and* $(\mu\text{-}SH)_2$-based $1a_1$ MOs of **III** (Fig. 4) giving a 3 centre–4 electron combination.

In EHMO theory it is possible to run the calculations with some or all overlap integrals $\langle\phi_i|\phi_j\rangle$ between atomic orbitals $\phi$ of certain atoms deleted (set to zero). Comparison of these results with those in which all orbital overlaps are taken into account allows one to estimate the importance of specific interactions. Therefore to check for the effects of direct repulsion between the alkyne $C_{ac}$ carbons and $(\mu\text{-}SH)_2$ sulfurs we undertook a series of new calculations on **I**, **II** and **IV** with all the orbital overlaps $\langle C_{ac}|\mu\text{-}\underline{S}H\rangle$ set to zero. The results are summarized in Fig. 5.

For all three models there is a destabilising effect arising from $C_{ac}$–$(\mu\text{-}\underline{S}H)_2$ repulsive interactions and these increase in the sequence **I** < **II** < **IV** as the $C_{ac}\cdots S$ distance decreases. Regardless of whether the $\langle C_{ac}|\mu\text{-}\underline{S}H\rangle$ overlaps are set to zero, the perpendicular bridged geometry **II** is between *ca.* 2.5 and 4.0 eV less stable than the parallel bridged alternative, **I**. The energy of the tightly-bound alkyne complex **IV** stabilises relative to that of **II** *only* when the $\langle C_{ac}|\mu\text{-}\underline{S}H\rangle$ overlaps are set to zero, thus reflecting the improved metal–alkyne bonding. However, when the $C_{ac}\cdots S$ repulsive interactions are included there is a net destabilisation from **II** to **IV**.

**Concluding remarks.** The EHMO calculations show that in all instances parallel bonding of the alkyne in the complexes $[Mo_2(\mu\text{-}C_2H_2)(\mu\text{-}S)(\mu\text{-}SH)_2Cp_2]$ is preferred to the alternative perpendicular mode. The main origins are less effective metal–alkyne π(||) and π*(||) interactions in the perpendicular bridging mode due to the energetic and spatial disposition of the frontier orbitals of the fragment $[Mo_2(\mu\text{-}S)(\mu\text{-}SH)_2Cp_2]$ **III**. In addition, $C_{ac}\cdots S$ repulsive interactions are increased in the perpendicular bridged geometry, and these become even more prohibitive as the metal–alkyne distance is decreased.

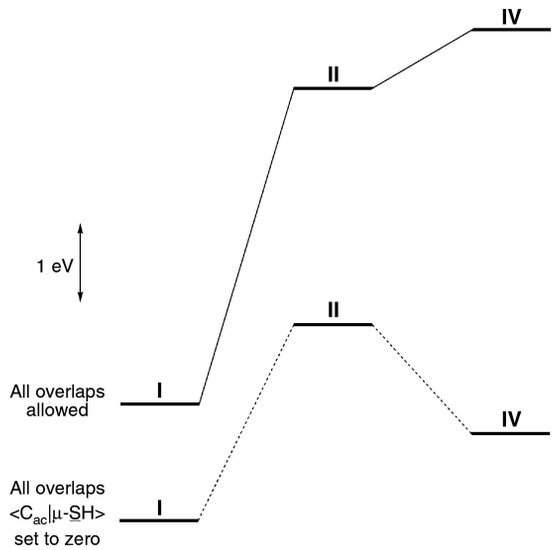


**Fig. 5** The relative total energies (sum of one electron orbital energies) of $[Mo_2(\mu\text{-}\eta^1,\eta^1\text{-}C_2H_2)(\mu\text{-}S)(\mu\text{-}SH)_2Cp_2]$ **I**, $[Mo_2(\mu\text{-}\eta^2,\eta^2\text{-}C_2H_2)(\mu\text{-}S)(\mu\text{-}SH)_2Cp_2]$ ($Mo_2\cdots C_2 = 2.00$ Å) **II** and $[Mo_2(\mu\text{-}\eta^2,\eta^2\text{-}C_2H_2)(\mu\text{-}S)(\mu\text{-}SH)_2Cp_2]$ ($Mo_2\cdots C_2 = 1.54$ Å) **IV**. Upper levels (joined by solid lines): all orbital interactions allowed. Lower levels (joined by dotted lines): all orbital overlaps $\langle C_{ac}|\mu\text{-}\underline{S}H\rangle$ set to zero.

### Cluster formation reactions of 2 with ruthenium carbonyl

We have previously shown that compounds of the type $[Mo_2(\mu\text{-}S)_2(\mu\text{-}SR)_2Cp_2]$ **3** react with $[Ru_3(CO)_{12}]$ to afford tetrahedral clusters of the type $[Mo_2Ru_2(\mu_3\text{-}S)_2(\mu\text{-}SR)_2(CO)_4Cp_2]$ **5**, in which one of the thiolate ligands has migrated to the Ru–Ru edge.[4] Similarly $[Mo_2(\mu\text{-}S)_2(\mu\text{-}SR)(\mu\text{-}PPh_2)Cp_2]$ **4** produced the analogous cluster $[Mo_2Ru_2(\mu_3\text{-}S)_2(\mu\text{-}SR)(\mu\text{-}PPh_2)(CO)_4Cp_2]$ **6** in which the thiolate ligand had again migrated while the phosphido group remained on the Mo–Mo edge (Scheme 2).[6]

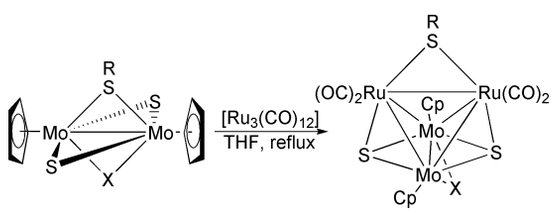


**3**: X = SR
**4**: X = $PPh_2$
**5**: X = SR
**6**: X = $PPh_2$

**Scheme 2** Synthesis of molybdenum–ruthenium clusters from complexes **3** and **4**.[4,6]

The reaction of **2** with $[Ru_3(CO)_{12}]$ was therefore examined, since in principle the alkyne ligand is also capable of assisting cluster assembly by donation to an additional metal in the same way as the sulfur atoms in **3** and **4**.

Separate reactions of **2a** and **2b** with $[Ru_3(CO)_{12}]$ were carried out in refluxing toluene for 2 h. In each case the same major product, $[Mo_2Ru_2(\mu_3\text{-}C_2Ph_2)(\mu_3\text{-}S)(\mu\text{-}SPr^i)_2(CO)_4Cp_2]$ **7** was formed in moderate to good yield (up to 62%), accompanied by a minor product $[Mo_2Ru(\mu\text{-}C_2Ph_2)(\mu_3\text{-}S)_2(CO)_3Cp_2]$ **8** (Scheme 3).

Incorporation of two $Ru(CO)_2$ units in **7** was confirmed by the IR and mass spectra. The $^1H$ NMR spectrum confirmed that the diphenylacetylene ligand had been retained, and showed inequivalent Cp ligands; the two $Pr^i$ groups are also inequivalent, as are the two methyl groups of each one. Similarly in the $^{13}C$ NMR spectrum the four carbonyl ligands are all inequivalent. These features mirror those observed in the related clusters **5** and **6**.

Crystals of **7** were grown by diffusion of methanol and ether into a dicholoromethane solution; the compound evidently

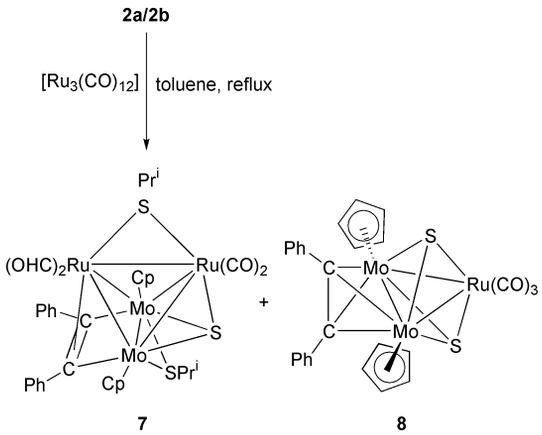


**Scheme 3** Synthesis of clusters **7** and **8**.

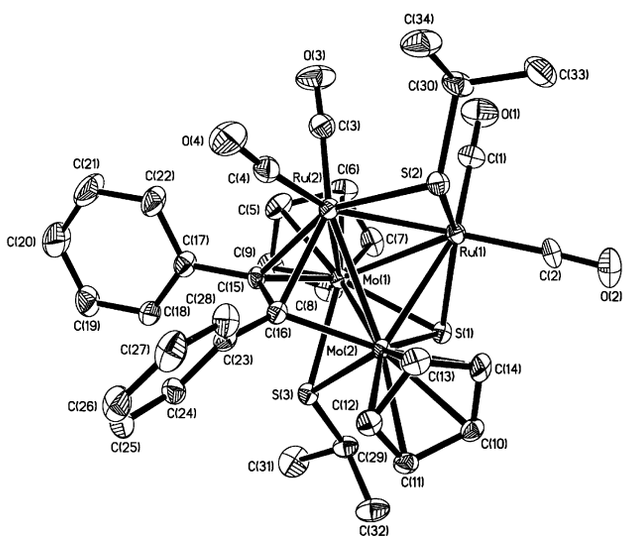


**Fig. 6** Molecular structure of $[Mo_2Ru_2(\mu_3\text{-}C_2Ph_2)(\mu_3\text{-}S)(\mu\text{-}SPr^i)_2(CO)_4Cp_2]$ **7** in the crystal showing the atomic numbering scheme. The methanol and water of solvation have been omitted.

crystallises as a solvate with MeOH and $0.5H_2O$ in the lattice, the latter presumably arising as an impurity in the methanol. The structure is shown in Fig. 6 with selected bond lengths and angles collected in Table 3. The metal framework consists of a distorted tetrahedron of two molybdenum and two ruthenium atoms, with the intermetallic distances similar to those in the related clusters **5** and **6**, though it is noticeable that here the $Ru_2$ unit is asymmetrically placed in relation to the $Mo_2$ core: Ru(1) is closer to Mo(2) whereas Ru(2) is closer to Mo(1). The Mo–Mo edge is bridged by one of the thiolate ligands, and as expected the other has migrated to the Ru–Ru edge; in contrast to the situation in **5** and **6** however, this latter thiolate ligand is somewhat asymmetrically coordinated. The Mo(1)–Mo(2)–Ru(1) face is capped by the sulfido ligand, whereas the Mo(1)–Mo(2)–Ru(2) face is occupied by the alkyne ligand, which is bonded in the $\mu_3$-|| mode often observed in metal clusters.[23] The torsion angle between the Mo(1)–Mo(2) bond and the alkyne C(15)–C(16) bond is 2.5°, very similar to that in **2**. The planar arrangement of the two Mo atoms, the alkyne carbons and S(1) is thus retained. The formation of a product analogous to **5** thus strengthens the analogy between the μ-S ligand in **3** and the $\mu\text{-}C_2Ph_2$ in **2**.

Complex **8** was also characterised by spectroscopy and X-ray structure determination. Incorporation of ruthenium was indicated by its IR spectrum, where a pattern typical of a $Ru(CO)_3$ unit was observed. This complex showed no $Pr^i$ groups in its $^1H$ NMR spectrum, and a very symmetrical structure was indicated by the equivalence of the phenyl groups and the Cp ligands. A change in the bonding mode for the alkyne ligand

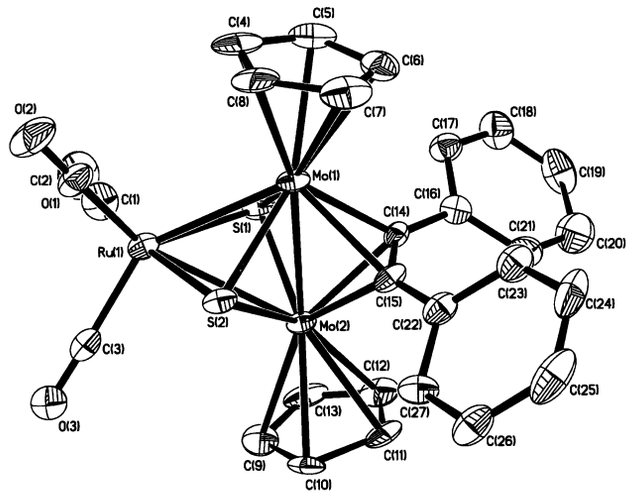


**Fig. 7** Molecular structure of $[Mo_2Ru(\mu\text{-}C_2Ph_2)(\mu_3\text{-}S)_2(CO)_3Cp_2]$ **8** in the crystal showing the atomic numbering scheme.

was indicated by the fact that the $^{13}C$ NMR shift of the alkyne carbons appeared at $\delta$ 67.5, a change of almost 200 ppm compared to **2** and similar to that seen in **1**. Small crystals suitable for diffraction were grown from a solution in $CH_2Cl_2$ and light petroleum at 4 °C. The unit cell contains two independent molecules which are structurally very similar. The structure of one of these is depicted in Fig. 7, with selected bond lengths and angles given in Table 4. The molecule consists of a triangle of metal atoms in which the Mo–Mo bond is rather short [2.5860(9) Å] whereas the Mo–Ru bonds are towards the longer end of the range observed for such bonds. The ruthenium atom bears three terminal CO ligands and each Mo atom its Cp ligand. The metal triangle is bridged above and below the plane by two $\mu_3$-sulfido ligands; the Ru–$\mu_3$-S bonds are significantly longer than those found in **5**–**7** and in other Mo/Ru/S clusters such as $[Mo_2Ru(\mu_3\text{-}S)(CO)_7Cp_2]$[24] and $[Mo_2Ru_2(\mu_3\text{-}S)_2(CO)_8(\eta\text{-}C_5H_4CO_2Me)_2]$.[25] In addition the Mo–Mo edge is bridged by the diphenylacetylene ligand, which has now reverted to a perpendicular orientation: the torsion angle between the Mo(1)–Mo(2) bond and the C(14)–C(15) bond is 85.6° in the molecule shown and 87.6° in the other. If this ligand is considered to be a four electron donor, the compound is an electron-precise 48-electron cluster. The mechanism of formation of **8** is clearly rather more complex than that of **7** in that further dealkylation of at least one of the thiolate ligands in **2**, and the loss of one other sulfur, is required during the reaction. It is interesting to note, however, that we do not see any evidence of such further dealkylation in the reactions of **3** and **4** with $[Ru_3(CO)_{12}]$ under identical conditions.

## Conclusions

We have synthesized the first dinuclear complex of a Group 6 metal to contain an alkyne ligand coordinated in the $\mu\text{-}\eta^1,\eta^1$ (dimetallacyclobutene) bonding mode, in which the C–C axis lies parallel to the metal–metal bond. Molecular orbital calculations have shown that this bonding mode provides better overlap with metal orbitals, coupled with reduced repulsion with the lone pairs of the bridging thiolates. It is clear, however, that obtaining compounds of this type is dependent on a fine balance of steric (and maybe electronic) factors involving the substituents on both the alkyne and the thiol; for example, the reaction of **1** with EtSH produced only the two isomers of the known complex $[Mo_2(\mu\text{-}S)_2(\mu\text{-}SEt)_2Cp_2]$ in a combined yield of 38%. We have also shown that complex **2** can participate in cluster building reactions by coordination of additional ruthenium carbonyl fragments in a manner similar to that of the sulfido-bridged species **3**. Further investigations of the reactivity of the alkyne ligand in **2** are currently in progress.

**Table 3** Selected bond lengths [Å] and angles [°] for complex **7**

| | | | |
|---|---|---|---|
| Mo(1)–C(15) | 2.146(5) | Mo(1)–S(1) | 2.3504(14) |
| Mo(1)–S(3) | 2.4592(15) | Mo(1)–Mo(2) | 2.7138(6) |
| Mo(1)–Ru(2) | 2.7330(6) | Mo(1)–Ru(1) | 2.8273(6) |
| Mo(2)–C(16) | 2.136(5) | Mo(2)–S(1) | 2.3773(14) |
| Mo(2)–S(3) | 2.4680(13) | Mo(2)–Ru(1) | 2.7997(7) |
| Mo(2)–Ru(2) | 2.8687(6) | Ru(1)–C(1) | 1.892(6) |
| Ru(1)–C(2) | 1.902(6) | Ru(1)–S(1) | 2.3277(14) |
| Ru(1)–S(2) | 2.3299(15) | Ru(1)–Ru(2) | 2.6876(6) |
| Ru(2)–C(3) | 1.882(7) | Ru(2)–C(4) | 1.914(6) |
| Ru(2)–C(15) | 2.176(5) | Ru(2)–C(16) | 2.213(6) |
| Ru(2)–S(2) | 2.3520(14) | O(1)–C(1) | 1.144(8) |
| O(2)–C(2) | 1.142(8) | O(3)–C(3) | 1.157(8) |
| O(4)–C(4) | 1.149(8) | C(15)–C(16) | 1.432(8) |
| | | | |
| C(15)–Mo(1)–S(3) | 72.08(15) | S(1)–Mo(1)–S(3) | 76.67(5) |
| C(15)–Mo(1)–Mo(2) | 72.46(14) | Mo(2)–Mo(1)–Ru(2) | 63.560(17) |
| Mo(2)–Mo(1)–Ru(1) | 60.655(16) | Ru(2)–Mo(1)–Ru(1) | 57.780(16) |
| C(16)–Mo(2)–S(3) | 73.56(15) | S(1)–Mo(2)–S(3) | 76.02(5) |
| C(16)–Mo(2)–Mo(1) | 72.67(15) | Mo(1)–Mo(2)–Ru(1) | 61.677(16) |
| Mo(1)–Mo(2)–Ru(2) | 58.545(16) | Ru(1)–Mo(2)–Ru(2) | 56.591(16) |
| S(1)–Ru(1)–S(2) | 139.94(5) | Ru(2)–Ru(1)–Mo(2) | 63.000(17) |
| Ru(2)–Ru(1)–Mo(1) | 59.350(16) | Mo(2)–Ru(1)–Mo(1) | 57.668(15) |
| C(15)–Ru(2)–C(16) | 38.1(2) | Ru(1)–Ru(2)–Mo(1) | 62.871(17) |
| Ru(1)–Ru(2)–Mo(2) | 60.409(16) | Mo(1)–Ru(2)–Mo(2) | 57.895(16) |
| Ru(1)–S(1)–Mo(1) | 74.36(4) | Ru(1)–S(1)–Mo(2) | 73.02(4) |
| Mo(1)–S(1)–Mo(2) | 70.06(4) | Ru(1)–S(2)–Ru(2) | 70.06(4) |
| Mo(1)–S(3)–Mo(2) | 66.84(4) | O(1)–C(1)–Ru(1) | 179.1(6) |
| O(2)–C(2)–Ru(1) | 177.1(6) | O(3)–C(3)–Ru(2) | 177.7(6) |
| O(4)–C(4)–Ru(2) | 174.9(6) | C(16)–C(15)–Mo(1) | 107.2(4) |
| C(16)–C(15)–Ru(2) | 72.4(3) | Mo(1)–C(15)–Ru(2) | 78.44(18) |
| C(15)–C(16)–Mo(2) | 107.6(4) | C(15)–C(16)–Ru(2) | 69.6(3) |
| Mo(2)–C(16)–Ru(2) | 82.52(19) | | |

**Table 4** Selected bond lengths [Å] and angles [°] for the illustrated molecule of complex **8**

| | | | |
|---|---|---|---|
| Ru(1)–C(3) | 1.908(9) | Ru(1)–C(1) | 1.911(9) |
| Ru(1)–C(2) | 1.925(8) | Ru(1)–S(1) | 2.392(2) |
| Ru(1)–S(2) | 2.398(2) | Ru(1)–Mo(1) | 2.8819(10) |
| Ru(1)–Mo(2) | 2.9337(10) | Mo(1)–C(14) | 2.119(7) |
| Mo(1)–C(15) | 2.205(7) | Mo(1)–S(1) | 2.3596(19) |
| Mo(1)–S(2) | 2.373(2) | Mo(1)–Mo(2) | 2.5860(9) |
| Mo(2)–C(15) | 2.137(8) | Mo(2)–C(14) | 2.176(7) |
| Mo(2)–S(1) | 2.3472(19) | Mo(2)–S(2) | 2.3847(19) |
| O(1)–C(1) | 1.118(9) | O(2)–C(2) | 1.146(9) |
| O(3)–C(3) | 1.137(9) | C(14)–C(15) | 1.359(9) |
| | | | |
| C(3)–Ru(1)–C(1) | 94.1(4) | C(3)–Ru(1)–C(2) | 103.9(3) |
| C(1)–Ru(1)–C(2) | 93.9(4) | C(3)–Ru(1)–S(1) | 128.1(2) |
| C(1)–Ru(1)–S(1) | 80.6(3) | C(2)–Ru(1)–S(1) | 127.9(3) |
| C(3)–Ru(1)–S(2) | 91.3(2) | C(1)–Ru(1)–S(2) | 173.3(3) |
| C(2)–Ru(1)–S(2) | 88.8(2) | S(1)–Ru(1)–S(2) | 92.92(7) |
| Mo(1)–Ru(1)–Mo(2) | 52.79(2) | C(14)–Mo(1)–S(1) | 74.94(19) |
| C(15)–Mo(1)–S(1) | 100.28(19) | C(14)–Mo(1)–S(2) | 102.69(19) |
| C(15)–Mo(1)–S(2) | 74.8(2) | S(1)–Mo(1)–S(2) | 94.40(6) |
| Mo(2)–Mo(1)–Ru(1) | 64.63(3) | C(15)–Mo(2)–S(1) | 102.7(2) |
| C(14)–Mo(2)–S(1) | 74.18(19) | C(15)–Mo(2)–S(2) | 75.8(2) |
| C(14)–Mo(2)–S(2) | 100.59(18) | S(1)–Mo(2)–S(2) | 94.41(7) |
| Mo(1)–Mo(2)–Ru(1) | 62.58(2) | Mo(2)–S(1)–Mo(1) | 66.65(5) |
| Mo(2)–S(1)–Ru(1) | 76.49(6) | Mo(1)–S(1)–Ru(1) | 74.68(5) |
| Mo(1)–S(2)–Mo(2) | 65.85(5) | Mo(1)–S(2)–Ru(1) | 74.31(6) |
| Mo(2)–S(2)–Ru(1) | 75.66(6) | O(1)–C(1)–Ru(1) | 177.8(9) |
| O(2)–C(2)–Ru(1) | 179.1(9) | O(3)–C(3)–Ru(1) | 177.0(7) |
| Mo(1)–C(14)–Mo(2) | 74.0(2) | Mo(2)–C(15)–Mo(1) | 73.1(2) |

## Experimental

General experimental techniques were as described in a recent paper from this laboratory.[26] Infrared spectra were recorded in dichloromethane solution on a Perkin-Elmer 1600 FT-IR machine. $^{1}H$ and $^{13}C$ NMR spectra were obtained in $CDCl_3$ solution on a Bruker AC250 machine with automated sample-changer or an AMX400 spectrometer. Chemical shifts are given on the $\delta$ scale relative to $SiMe_4$ = 0.0 ppm. The $^{13}C\{^{1}H\}$ NMR spectra were routinely recorded using an attached proton test technique (JMOD pulse sequence). Mass spectra were recorded on a Fisons/BG Prospec 3000 instrument operating in fast atom bombardment mode with *m*-nitrobenzyl alcohol as matrix. Elemental analyses were carried out by the Microanalytical Service of the Department of Chemistry. Light petroleum refers to the fraction boiling in the range 60–80 °C.

The complex $[Mo_2(\mu\text{-}C_2Ph_2)(CO)_4Cp_2]$ **1** was prepared by heating $[Mo_2(CO)_6Cp_2]$ with diphenylacetylene in refluxing octane for 2.5 h,[27] or by the reaction of $[Mo_2(CO)_4Cp_2]$ (prepared *in situ* by decarbonylation of $[Mo_2(CO)_6Cp_2]$) with diphenylacetylene in refluxing toluene; the yield was 60–70% by both methods.

**Table 5** Summary of crystallographic data for complexes **2a**, **7**·MeOH·0.5$H_2O$ and **8**

| | **2a** | **7**·MeOH·0.5$H_2O$ | **8** |
|---|---|---|---|
| Empirical formula | $C_{30}H_{34}Mo_2S_3$ | $C_{35}H_{39}Mo_2O_{5.50}Ru_2S_3$ | $C_{27}H_{20}Mo_2O_3RuS_2$ |
| Formula weight | 682.63 | 1037.86 | 749.50 |
| $T$/K | 150(2) | 150(2) | 150(2) |
| Crystal system | Monoclinic | Monoclinic | Monoclinic |
| Space group | $P2_1/n$ | $C2/c$ | $C2/c$ |
| $a$/Å | 10.2162(7) | 9.7777(5) | 34.187(6) |
| $b$/Å | 24.5292(16) | 23.9675(14) | 7.8516(13) |
| $c$/Å | 11.6041(8) | 32.4670(18) | 41.618(7) |
| $\beta$/° | 91.8910(10) | 97.8980(10) | 113.969(3) |
| $V$/Å$^3$ | 2906.3(3) | 7536.4(7) | 10208(3) |
| $Z$ | 4 | 8 | 16 |
| $\mu$/mm$^{-1}$ | 1.096 | 1.643 | 1.744 |
| Reflections collected | 13949 | 22828 | 31674 |
| Independent reflections | 6663 [$R$(int) = 0.1504] | 8976 [$R$(int) = 0.0892] | 12319 [$R$(int) = 0.1272] |
| Final $R1$, $wR2$ [$I > 2\sigma(I)$] | 0.0630, 0.1842 | 0.0553, 0.1200 | 0.0570, 0.0945 |
| (all data) | 0.0908, 0.2401 | 0.0693, 0.1266 | 0.1257, 0.1110 |

### Synthesis of [$Mo_2(\mu\text{-}\eta^1,\eta^1\text{-}C_2Ph_2)(\mu\text{-}S)(\mu\text{-}SPr^i)_2Cp_2$] 2

A solution of [$Mo_2(\mu\text{-}C_2Ph_2)(CO)_4Cp_2$] **1** (1.2 g, 1.96 mmol) in toluene (150 cm$^3$) was treated with 5 equivalents of $Pr^iSH$ (0.9 cm$^3$, 9.69 mmol) and then heated to reflux for 18 h. The solvent was removed under vacuum, and the residue absorbed on a small amount of silica which was then loaded onto a chromatography column. Elution with light petroleum–$CH_2Cl_2$ (4 : 1) afforded a brown band of the symmetrical isomer of [$Mo_2(\mu\text{-}\eta^1,\eta^1\text{-}C_2Ph_2)(\mu\text{-}S)(\mu\text{-}SPr^i)_2Cp_2$] **2a** (263 mg, 19.7%). Further elution with a 3 : 1 mixture of the same solvents produced a dark purple zone of the unsymmetrical isomer **2b** (268 mg, 20%). Continued elution with firstly a 3 : 2 and then a 1 : 4 mixture of the same solvents produced two purple bands which were identified as the two isomers of [$Mo_2(\mu\text{-}S)_2(\mu\text{-}SPr^i)_2Cp_2$] (combined yield 91 mg, 8%).

Data for **2a**: Mp 177–179 °C. $^1$H NMR: $\delta$ 7.06–6.57 (m, 10 H, Ph), 5.88 (s, 10 H, Cp), 1.69 (septet, $J$ = 7 Hz, 2 H, CH) and 0.93 (d, $J$ = 7 Hz, 12 H, Me). $^{13}$C NMR: $\delta$ 242.4 (s, CPh), 154.9 (s, $C_{ipso}$), 137.4–123.3 (m, Ph), 98.3 (s, Cp), 46.9 (s, CH) and 26.8 (s, Me). (Found: C, 52.76; H, 5.56; S, 13.12. Calc. for $C_{30}H_{34}Mo_2S_3$: C, 52.79; H, 4.99; S, 14.08%). MS: $m/z$ 681, 638, 596 ($M^+ - n$Pr$^i$ where $n$ = 0–2).

Data for **2b**: Mp 192–194 °C. $^1$H NMR: $\delta$ 7.08–6.50 (m, 10 H, Ph), 5.99 (s, 10 H, Cp), 2.95 (septet, $J$ = 7 Hz, 1 H, CH), 1.84 (septet, $J$ = 7 Hz, 1 H, CH), 1.04 (d, $J$ = 7 Hz, 6 H, Me) and 0.92 (d, $J$ = 7 Hz, 6 H, Me). $^{13}$C NMR: $\delta$ 254.3 (s, *C*Ph), 154.4 ($C_{ipso}$), 134.9–121.8 (m, Ph), 98.4 (s, Cp), 42.2 (s, CH), 41.1 (s, CH), 26.5 (s, Me) and 26.1 (s, Me). (Found: C, 50.89; H, 4.90; S, 13.79. Calc. for $C_{30}H_{34}Mo_2S_3$·0.5$CH_2Cl_2$: C, 50.51; H, 4.83; S, 13.25%). MS: $m/z$ 682, 639, 598 ($M^+ - n$Pr$^i$ where $n$ = 0–2).

### Synthesis of [$Mo_2Ru_2(\mu_3\text{-}C_2Ph_2)(\mu_3\text{-}S)(\mu\text{-}SPr^i)_2(CO)_4Cp_2$] 7 and [$Mo_2Ru(\mu\text{-}C_2Ph_2)(\mu_3\text{-}S)_2(CO)_3Cp_2$] 8

A solution of **2a** (258.3 mg, 0.38 mmol) and [$Ru_3(CO)_{12}$] (240.2 mg, 0.38 mmol) in toluene (125 cm$^3$) was heated to reflux for 2.5 h with monitoring by spot TLC. After this time the solvent was removed and the residue chromatographed. After removal of a small amount of residual ruthenium carbonyl with light petroleum, the eluent was changed to a mixture of light petroleum–$CH_2Cl_2$ (17 : 3) which developed two closely spaced bands. The first of these, comprising the brown cluster **8**, was eluted in this solvent mixture (44.3 mg, 15.6%). Elution with a 4 : 1 mixture of the same solvents then produced the red–brown band of cluster **7** (90.2 mg, 23.9%).

An analogous reaction of **2b** (221.4 mg, 0.325 mmol) with [$Ru_3(CO)_{12}$] (220.7 mg, 0.345 mmol) afforded 29.7 mg (12.2%) of **8** and 200.8 mg (61.9%) of **7**.

Data for **7**: Mp 268–270 °C. IR($CH_2Cl_2$): 1998m, 1979s, 1946m and 1911w cm$^{-1}$. $^1$H NMR: $\delta$ 7.58–6.57 (m, 10 H, Ph), 5.45 (s, 5 H, Cp), 5.02 (s, 5 H, Cp), 2.80 (septet, $J$ = 7 Hz, 1 H, CH), 2.51 (septet, $J$ = 7 Hz, 1 H, CH), 1.54 (d, $J$ = 7 Hz, 3 H, Me), 1.46 (d, $J$ = 7 Hz, 3 H, Me), 1.43 (d, $J$ = 7 Hz, 3 H, Me) and 1.14 (d, $J$ = 7 Hz, 3 H, Me). $^{13}$C NMR: $\delta$ 225.4, 208.2, 206.6, 205.3 (CO), 201.4, 199.5 (*C*Ph), 153.2, 151.3 ($C_{ipso}$), 129.3–124.6 (m, Ph), 100.3, 94.2 (Cp), 61.1, 47.1 (CH), 28.0, 26.8, 26.1, 25.8 (Me). (Found: C, 40.48; H, 3.41; S, 9.74. Calc. for $C_{34}H_{34}Mo_2O_4Ru_2S_3$: C, 40.96; H, 3.41; S, 9.64%). MS: $m/z$ 998 ($M^+$).

Data for **8**: Mp 252–257 °C (decomp.). IR ($CH_2Cl_2$): 2041s and 1981m cm$^{-1}$. $^1$H NMR: $\delta$ 7.34–7.07 (m, 10 H, Ph), 5.23 (s, 10 H, Cp). $^{13}$C NMR: $\delta$ 199.7 (CO), 147.1 ($C_{ipso}$), 129.3, 128.1, 125.2 (Ph), 97.6 (Cp), 67.5 (*C*Ph). (Found: C, 43.48; H, 3.09; S, 8.38. Calc. for $C_{27}H_{20}Mo_2O_3RuS_2$: C, 43.26; H, 2.67; S, 8.54%). MS: $m/z$ 754 ($M^+$), 722 ($M^+ - S$).

### Crystal structure determinations of 2a, 7 and 8

Details of the crystal structure determinations are given in Table 5. The crystal of **7** contains MeOH and 50% $H_2O$ occupying a special position. Data collected were measured on a Bruker Smart CCD area detector with an Oxford Cryosystems low temperature system. The general procedures for structure solution were as described in a recent paper.[3] Complex scattering factors were taken from the program package SHELXTL[28] as implemented on the Viglen Pentium computer.

CCDC reference numbers 165393–165395.

See http://www.rsc.org/suppdata/dt/b1/b103698j/ for crystallographic data in CIF or other electronic format.

### Computational details for MO calculations

Molecular orbital calculations were performed using a modified extended-Hückel method employing weighted $H_{ij}$ values.[15] The fragment and molecular geometries were idealised to $C_{2v}$, but unless stated otherwise bond lengths and angles were based on those for the crystal structure of **2a**. All EHMO calculations were performed using the CACAO package[29] using the atomic parameters within the program. These gave satisfactory net atomic charges in all the molecules and fragments studied.

## References


1 T. Kabe, A. Ishihara and W. Qian, *Hydrodesulfurization and Hydrodenitrogenation*, Wiley/VCH, New York, 2000; *Transition Metal Sulfur Chemistry: Biological and Industrial Significance,* eds. E. I. Stiefel and K. Matsumoto, ACS Symposium Series, 1996, vol. 653.

2 U. Riaz, O. J. Curnow and M. D. Curtis, *J. Am. Chem. Soc.*, 1994, **116**, 4357; M. D. Curtis, U. Riaz, O. J. Curnow, J. W. Kampf, A. L. Rheingold and B. S. Haggerty, *Organometallics*, 1995, **14**, 5337.

3 H. Adams, N. A. Bailey, S. R. Gay, T. Hamilton and M. J. Morris, *J. Organomet. Chem.*, 1995, **493**, C25; H. Adams, A. Biebricher, S. R. Gay, T. Hamilton, P. E. McHugh, M. J. Morris and M. J. Mays, *J. Chem. Soc., Dalton Trans.*, 2000, 2983.
4 H. Adams, N. A. Bailey, S. R. Gay, L. J. Gill, T. Hamilton and M. J. Morris, *J. Chem. Soc., Dalton Trans.*, 1996, 2403.
5 M. Rakowski Dubois, M. C. VanDerveer, D. L. Dubois, R. C. Haltiwanger and W. K. Miller, *J. Am. Chem. Soc.*, 1980, **102**, 7456; H. Brunner, W. Meier, J. Wachter, P. Weber, M. L. Ziegler, J. H. Enemark and C. G. Young, *J. Organomet. Chem.*, 1986, **309**, 313.
6 H. Adams, N. A. Bailey, A. P. Bisson and M. J. Morris, *J. Organomet. Chem.*, 1993, **444**, C34; H. Adams, N. A. Bailey, M. N. Bancroft, A. P. Bisson and M. J. Morris, *J. Organomet. Chem.*, 1997, **542**, 131.
7 H. Adams, M. N. Bancroft and M. J. Morris, *Chem. Commun.*, 1997, 1445; H. Adams, C. Allott, M. N. Bancroft and M. J. Morris, *J. Chem. Soc., Dalton Trans.*, 2000, 4145.
8 H. Adams, C. Allott, M. N. Bancroft and M. J. Morris, *J. Chem. Soc., Dalton Trans.*, 1998, 2607.
9 W. I. Bailey, Jr., M. H. Chisholm, F. A. Cotton and L. A. Rankel, *J. Am. Chem. Soc.*, 1978, **100**, 5764.
10 D. M. Hoffman, R. Hoffmann and C. R. Fisel, *J. Am. Chem. Soc.*, 1982, **104**, 3858.
11 J. Heck, K.-A. Kriebisch, W. Massa and S. Wocadlo, *J. Organomet. Chem.*, 1994, **482**, 81.
12 K. J. Ahmed, M. H. Chisholm, K. Folting and J. C. Huffman, *Organometallics*, 1986, **5**, 2171; M. J. Calhorda and R. Hoffmann, *Organometallics*, 1986, **5**, 2181; F. A. Cotton and X. Feng, *Inorg. Chem.*, 1990, **29**, 3187.
13 M. A. Chisholm and M. A. Lynn, *J. Organomet. Chem.*, 1998, **550**, 141.
14 P. Mountford, *J. Chem. Soc., Dalton Trans.*, 1994, 1843.
15 R. Hoffmann and W. N. Lipscomb, *J. Chem. Phys.*, 1962, **36**, 2179.
16 S. G. Bott, D. L. Clark, M. L. H. Green and P. Mountford, *J. Chem. Soc., Dalton Trans.*, 1991, 471 and references therein.
17 R. P. Aggarwal, N. G. Connelly, M. C. Crespo, B. J. Dunne, P. M. Hopkins and A. G. Orpen, *J. Chem. Soc., Dalton Trans.*, 1992, 655.
18 M. H. Chisholm, B. K. Conroy, D. L. Clark and J. C. Huffman, *Polyhedron*, 1988, **7**, 903.
19 D. L. DuBois, W. K. Miller and M. Rakowski DuBois, *J. Am. Chem. Soc.*, 1981, **103**, 3429.
20 W. Tremel, R. Hoffmann and E. D. Jemmis, *Inorg. Chem.*, 1989, **28**, 1213.
21 J. C. Green, M. L. H. Green, P. Mountford and M. J. Parkington, *J. Chem. Soc., Dalton Trans.*, 1990, 3407.
22 The United Kingdom Chemical Database Service, D. A. Fletcher, R. F. McMeeking and D. Parkin, *J. Chem. Inf. Comput. Sci.*, 1996, **36**, 746.
23 E. Sappa, A. Tiripicchio and P. Braunstein, *Chem. Rev.*, 1983, **83**, 203; P. R. Raithby and M. J. Rosales, *Adv. Inorg. Chem. Radiochem.*, 1985, **29**, 169.
24 R. D. Adams, J. E. Babin and M. Tasi, *Organometallics*, 1988, **7**, 219.
25 L.-C. Song, J.-Q. Wang, Q.-M. Hu and X.-Y. Huang, *Polyhedron*, 1996, **15**, 4295.
26 H. Adams, L. J. Gill and M. J. Morris, *Organometallics*, 1996, **15**, 464.
27 S. A. R. Knox, R. F. D. Stansfield, F. G. A. Stone, M. J. Winter and P. Woodward, *J. Chem. Soc., Dalton Trans.*, 1982, 173.
28 SHELXTL, An integrated system for solving and refining crystal structures from diffraction data (Revision 5.1), Bruker AXS Ltd, Madison, WI, 1997.
29 C. Mealli and D. M. Proserpio, *J. Chem. Educ.*, 1990, **67**, 3399.